The North African Journal of Scientific Publishing (NAJSP)
مجلة شمال إفريقيا للنشر العلمي (NAJSP)
E-ISSN: 2959-4820
Volume 3, Issue 4, 2025
Page No: 229-235
Website: https://najsp.com/index.php/home/index
SJIFactor 2024: 5.49 معامل التأثير العربي (AIF) 2025: 0.69 ISI 2024: 0.696

Stratigraphy of the Soil layers of Bosita Area using Ground Penetrating Radar

Ramadan E. Zaed[1], Khaled A. Bin Omar [2*]
[1,2]Faculty of Arts and Science, El Mergib University, Musallata, Libya

دراسة طبقات التربة في منطقة بوسيتا باستخدام الرادار المخترق للأرض

رمضان زايد[1]، خالد بن عمر[2*]
[1،2]كلية الآداب والعلوم، جامعة المرقب، مسلاته، ليبيا

*Corresponding author: rezaed@elmergib.edu.ly

Received: October 15, 2025	Accepted: December 23, 2025	Published: December 30, 2025

Abstract:
The application of Ground Penetrating Radar (GPR) remains a pivotal geophysical methodology for the non-invasive high-resolution imaging of pedogenic and lithological stratigraphy. This investigation delineates the subsurface architectural framework of a 1-hectare study site in the Bosita area, extending to a vertical depth of 22 meters. Utilizing a strategic survey grid, six geophysical profiles were executed, comprising four peripheral boundary transects and two internal diagonal intersections, encompassing a cumulative linear distance of 454 meters. Radargram acquisition was subjected to rigorous digital signal processing, employing advanced filtering algorithms to enhance the signal-to-noise ratio and resolve complex dielectric interfaces. The synthesized data facilitated a comprehensive interpretation of the phreatic zone (water table) depth and the elucidation of the stratigraphic sequence. Results reveal significant lateral and vertical heterogeneity, driven by pronounced lithofacies transitions within the sedimentary record. The interpretation identifies four distinct primary lithostratigraphic units attributable to recent Quaternary deposits. These findings underscore the efficacy of electromagnetic induction in mapping depositional facies and characterizing the structural complexity of Holocene-Pleistocene terrestrial successions.

Keywords: Ground Penetrating Radar (GPR), Subsurface stratigraphic imaging (Quaternary deposits), Water table (phreatic zone) delineation, Lithofacies heterogeneity.

الملخص:
تظل تقنية الرادار المخترق للأرض (GPR) منهجية جيوفيزيائية محورية للتصوير غير التدخلي وعالي الدقة للطباقية التربوية والليثولوجية. تهدف هذه الدراسة إلى تحديد الإطار الهيكلي لما تحت السطح لموقع دراسة تبلغ مساحته هكتاراً واحداً في منطقة "بوسيتيا"، وصولاً إلى عمق رأسي قدره 22 متراً. وباستخدام شبكة مسح استراتيجية، تم تنفيذ ستة مقاطع عرضية جيوفيزيائية، شملت أربعة مسارات محيطية ومسارين قطريين داخليين، بإجمالي مسافة خطية بلغت 454 متراً. خضعت البيانات الرادارية المكتسبة لمعالجة رقمية دقيقة للإشارات، حيث تم تطبيق خوارزميات ترشيح متقدمة لتعزيز نسبة الإشارة إلى الضوضاء وتوضيح الواجهات العازلة للكهرباء (dielectric interfaces) المعقدة. ساهمت البيانات المُصنّعة في تقديم تفسير شامل لعمق النطاق المشبع (مستوى الماء الأرضي) وتوضيح التتابع الطبقي. وتكشف النتائج عن تباين جانبي ورأسي ملحوظ ناتج عن تغيرات واضحة في السحنات الصخرية (lithofacies) ضمن السجل الرسوبي. وقد حدد التفسير أربع وحدات ليثوستراتيغرافية رئيسة متميزة تنتمي إلى رواسب العصر الرباعي الحديث. تؤكد هذه النتائج

فعالية الحث الكهرومغناطيسي في رسم خرائط السحنات الترسيبية وتوصيف التعقيد الهيكلي للتتابعات البرية التي تعود لعهدي الهولوسين والبليستوسين.

الكلمات المفتاحية: رادار اختراق الأرض (GPR)، تصوير الطبقات التحت سطحية (رواسب العصر الرباعي)، تحديد منسوب المياه الجوفية (المنطقة الفرياتيكية)، عدم تجانس السحنات الطبقية.

Introduction:

Ground Penetrating Radar (GPR) constitutes an advanced, high-resolution geophysical technique for the non-invasive characterization of shallow subsurface environments, including pedogenic horizons, lithified substrates, and cryospheric materials. Operating across the electromagnetic spectrum within approximately 10–1000 MHz, GPR enables the imaging of internal geological architectures that are otherwise difficult to resolve without intrusive sampling. The method involves transmitting short electromagnetic pulses into the ground and recording the travel-time and amplitude of reflected signals generated at contrasts in dielectric permittivity; the resulting radargrams provide laterally continuous datasets that support detailed interpretation of the near-surface stratigraphic framework.

Within sedimentary geology, GPR has become a principal diagnostic tool for high-fidelity stratigraphic reconstruction and facies analysis. As emphasized by Tatum and Francke (2012), near-continuous GPR profiles facilitate the delineation of complex stratigraphic architectures, the definition of sand-body morphology and geometries, and the quantification of internal sedimentary structures. This capacity for in situ visualization significantly enhances the mapping of depositional facies, bounding surfaces, and environmental transitions, offering a level of spatial detail that typically exceeds that achievable through point-based observations alone.

The progressive refinement of GPR systems has, therefore, shifted subsurface characterization from reliance on interpolation toward a paradigm of direct visualization. Traditionally, assessments of lateral continuity and unit correlations depended on integrating discrete evidence from boreholes, outcrops, or shallow excavations, approaches that often introduce interpretive uncertainty due to limited spatial coverage. Under favorable geophysical conditions, particularly in high-resistivity settings such as well-sorted sands and gravels, GPR can yield a coherent and continuous record of subsurface stratigraphy; as noted by Annan (2005), this capability effectively bridges the gaps between isolated observations and provides a more robust representation of geological heterogeneity and variability.

Site Description:

The study area is located near the coast of Tripoli City aside from Abosita Horse races yard at 32 54’ N and 13 13’ 15” E with an elevation of 30 m above sea level (Figure,1), covers an area of about (1 ha). The area is plane flat bounded by high building of five stores. The lithology of this region is dominated by Gargaresh Formation described by (Hlal, O and Bennur, S 2014), as calcarenite, including shell fragments and interbeded with occasional silty lenses.

Ground penetrating radar theory:

An ideal method for mapping shallow sub-surface features (<50m) is ground-penetrating radar (GPR). It has become widely popular since the mid-1990s for geophysical studies requiring a high vertical resolution, as well as allowing for real-time acquisition of the data (Neal 2004). One of the more common ways of collecting data is the common-off set technique, which means that the transmitting and receiving antennas are kept at a constant distance from each other and can be moved in any horizontal direction to collect data, such as the unit used in this study (Figure 2).

Figure (1): Study area location assigned by the four corners (A, B, C and D).

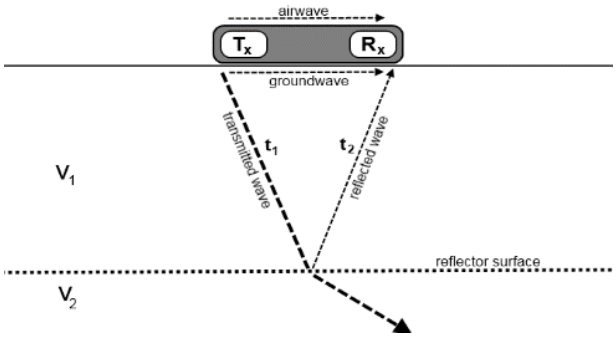

Figure (2): Illustration of the GPR-technique showing the transmitting (Tx) antenna and receiving (Rx) antenna of the unit as well as two media of different speeds (v_1 and v_2) in which the electromagnetic signal travels), t_1 is the time between transmission and reflection and t_2 is the time between reflection and reception (Molron, J.et al, 2020).

A GPR sends out an electromagnetic pulse and depending on the properties of the ground, reflective signals are recorded to indicate subsurface features. If the speed of the signal in the ground is known, a depth can be calculated from the time delay of the reflected signal. The velocity of the signal depends on the electromagnetic properties of the material in which it is propagates; mainly the relative electric permittivity (e), the electric conductivity (s) and the relative magnetic permeability (μr). When the unit transmits a pulse from the transmitting antenna (T) any reflected wave from the subsurface as well as air- and ground waves will be recorded by the receiving antenna (Rx) in the unit. The time between two transmitted pulses from the Tx is called the time-window (Tx). If a pulse reflects of a boundary or object, the time between transmission and reception is called the two-way travel time (TWT), and in the case illustrated in figure 2 TWT would be t_1+t_2.

Methodology:

Data Acquisition:

GPR data were acquired using a MALÅ unshielded antenna with a nominal central frequency of 100 MHz (Figure 3.1), coupled to an XV monitor operating under a Linux environment (Figures 3 and 2). This configuration enabled real-time visualization of radargrams in the field, allowing acquisition parameters to be adjusted as needed to optimize data quality. Throughout the survey, the unshielded antenna was towed manually at approximately walking pace, while the monitor unit was carried at the operator's torso to facilitate continuous observation. A measuring wheel was employed to ensure consistent distance calibration and uniform trace spacing along each traverse. Under favorable site conditions, the 100 MHz system provides a vertical resolution on the order of 0.50–0.60 m, supporting the detection of decimeter- to meter-scale stratigraphic variations. The survey approach builds upon a well-established technological lineage in subsurface electromagnetic prospecting, tracing from early applications in 1904, the introduction of pulsed techniques by 1926, and subsequent expansion to investigations of ice, sand, rock, coal, salt, and groundwater systems during the 1930s (Daniels, 2004). A constant time-window was maintained for all profiles to preserve acquisition consistency across the site and was judged in situ to provide an appropriate compromise between depth coverage and signal clarity. As illustrated in Figure 4, six profiles were executed across the study area, providing spatial coverage designed to capture the principal geomorphic and stratigraphic variations within the surveyed domain.

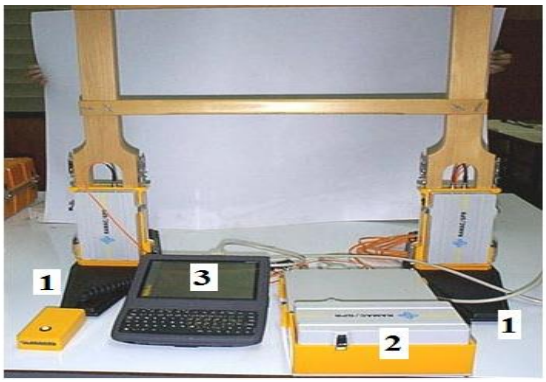

Figure (3): GPR setup for profiling (1) antenna (2) Controller and 3 PC.

Figure (4): Overview of the Six GPR profiles (shown as orange lines) scanned within study area.

Data Processing:

All acquired raw datasets were subjected to post-processing to enhance interpretability and facilitate robust stratigraphic analysis across the investigated profiles, consistent with standard practice in GPR investigations. In the unprocessed records, many deeper reflection events are weak or obscured, limiting direct geological interpretation. Although GPR processing can be undertaken in a highly comprehensive manner, the present study adopted a streamlined workflow comprising only fundamental processing steps, as more advanced procedures were not required to meet the study objectives or to interrogate deeper, more complex signal components. The overall processing sequence is summarized in Figure 5 and is detailed in the following section.

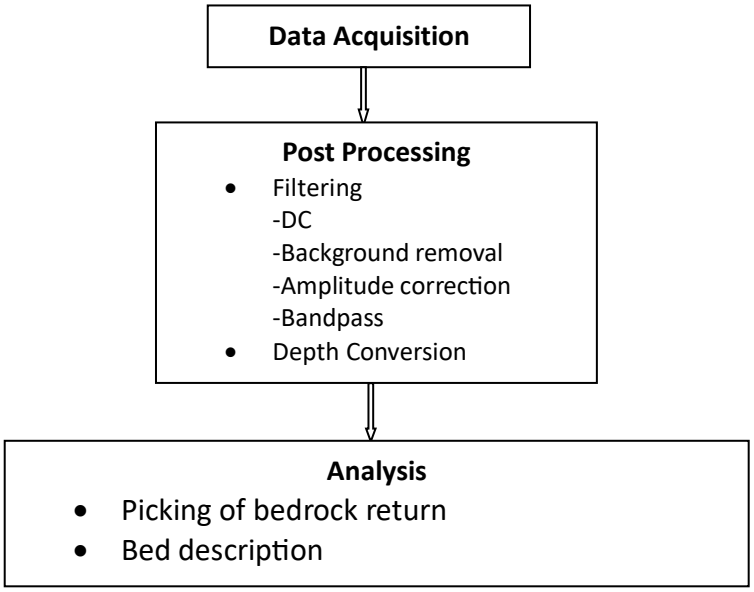

Figure (5): Schematic diagram of the work flow involved in acquisition, processing and interpretation of GPR data.

DC filtering was applied to remove the direct-current (DC) bias from each trace and center the signal about zero amplitude, followed by background removal to suppress coherent, trace-to-trace repetitive components associated with instrument noise and system ringing. Subsequently, amplitude correction was implemented through gain control to compensate for attenuation with depth; specifically, automatic gain control (AGC) was used to normalize amplitudes along the traces and enhance the continuity and visibility of deeper reflectors. Finally, bandpass filtering was performed to improve the signal-to-noise ratio by preserving the dominant frequency content of the subsurface reflections while attenuating low-frequency drift and high-frequency noise outside the selected passband.

Results and Interpretation:

Each profile is presented as a post-processed radargram, on which interpreted reflectors are superimposed. In all radargrams, the 0 m distance mark corresponds to the surface position along the profile. Prominent reflectors were systematically identified from the processed datasets and are represented by continuous, color-coded solid lines. Where relevant, arrows are used to highlight diagnostically significant features or anomalous targets.

The detailed interpretation of the radar profiles is provided in the subsequent sections. Figures 6–11 display the processed images of the surveyed profiles, illustrating the stratigraphic architecture of the sedimentary succession to the investigated depth (~22 m), in addition to indicating the depth to the water table. Notably, the number of resolvable beds differs among profiles, reflecting pronounced lateral facies variability within the sediment package. Across the entire study area, the most laterally persistent and distinctive unit occurs below approximately 2 m depth in all profiles; it is predominantly composed of pebbly sand and exhibits considerable thickness variability, typically ranging from about 2.5 to 5.0 m. Among the surveyed transects, Profile AC, extending from corner A to corner C, was selected as the representative section for reconstructing the stratigraphic sequence over the full surveyed depth.

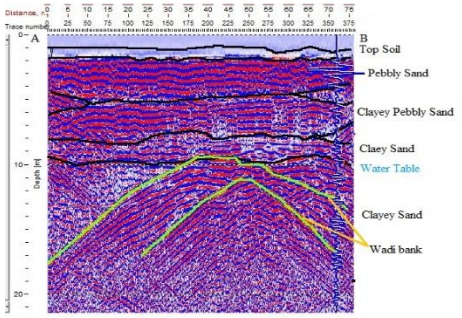

Figure (6): Processed data from profile AB (75 m long).

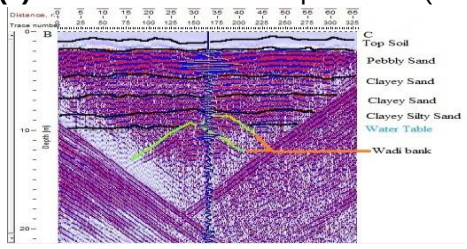

Figure (7): Processed data from profile BC (65 m long).

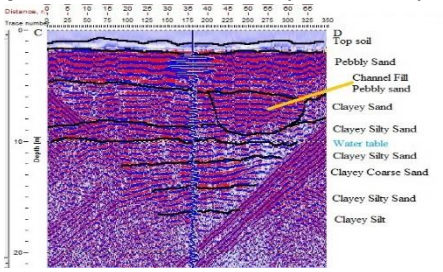

Figure (8): Processed data from profile CD (70 m long).

Four principal stratigraphic units are identifiable, arranged from top to bottom as follows: (i) a pebbly sand layer with an average thickness of approximately 2.5 m; (ii) an underlying clayey sand unit of about 4.75 m; (iii) a clayey silt layer approximately 4.5 m thick that locally grades into silty clay; and (iv) a basal clayey silty sand unit with a thickness on the order of 6.5 m. Notably, the thicknesses of these units are not laterally uniform; instead, they exhibit systematic thickening and thinning within the investigated interval, reflecting spatial variability in depositional conditions and sediment accommodation.

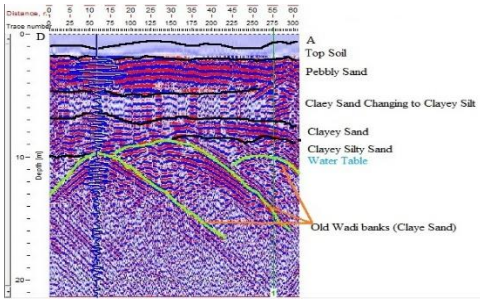

Figure (9): Processed data from profile DA (62 m long).

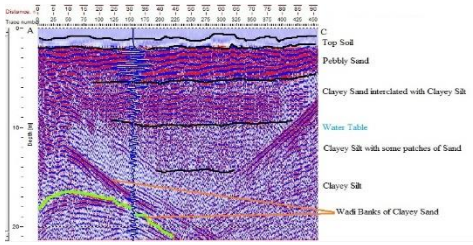

Figure (10): Processed data from profile AC (91 m long).

In Figures 9 and 10, the stratigraphic sections clearly exhibit an alternation between clayey sand and clayey silt units, with an upward transition across the profiles. These depositional units display variable thicknesses, characterized by both thickening and thinning trends with increasing depth, reflecting fluctuations in sediment supply and depositional energy during the investigated stratigraphic interval.

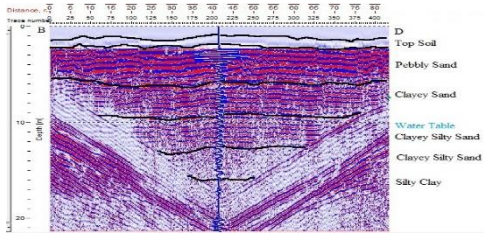

Figure (11): Processed data from profile BD (85 m long).

All surveyed profiles indicate the presence of interbedded silt and clay lenses within the identified stratigraphic units, reflecting pronounced facies variability in the deposited sediments and the localized influence of valley-derived sediment sources. Below approximately 10 m depth, distinct wadi bank boundaries (highlighted in yellow) are consistently detected at varying depths and lateral positions, delineating an infilled, buried palaeochannel. This geomorphic–stratigraphic signature suggests that the corresponding interval of the Gargaresh Formation was deposited under predominantly fluvial conditions.

Discussion:

The application of ground-penetrating radar (GPR) in the Bosita district demonstrates its strong capability for resolving shallow subsurface heterogeneity in unconsolidated Quaternary deposits. The high signal resolution obtained in the surveyed profiles allowed for clear identification of lithological contrasts, bed geometries, and structural controls, which are often difficult to capture using conventional invasive methods. In particular, the sensitivity of GPR to dielectric property variations enabled effective discrimination between coarse-grained (pebbly sand and sand) and fine-grained (clay and silt) sedimentary units, thereby providing a reliable framework for stratigraphic interpretation.

The observed variation in sediment thickness, ranging from 2.5 to 6.5 m within valley fills, reflects the combined influence of paleo-topography, fluvial dynamics, and post-depositional processes. The systematic thinning of sediments toward valley flanks is consistent with erosional truncation and reduced accommodation space away from the channel axes. This spatial pattern supports the interpretation of valley-controlled sedimentation, where maximum deposition occurred along paleo-channels, followed by lateral attenuation toward adjacent higher ground.

The identification of a distinct bedrock ridge in profiles AB, BC, DA, and AC is particularly significant, as it indicates a structural or geomorphological control on sediment distribution. This ridge effectively separates adjacent paleo-channels, suggesting that bedrock morphology played a key role in directing sediment transport and deposition during the late Quaternary. Such features likely influenced local hydrological regimes, including groundwater flow pathways and storage potential, by compartmentalizing sedimentary bodies with differing hydraulic properties.

At greater depths, the GPR sections reveal a highly complex internal stratigraphy marked by interbedded and lens-shaped clay, silt, and sand units. These heterolithic facies arrangements indicate rapid lateral and vertical facies changes, characteristic of dynamic depositional environments such as fluvial or fluvio-lacustrine systems. The presence of fine-grained lenses within coarser deposits suggests episodic low-energy conditions, possibly related to floodplain sedimentation, channel abandonment, or short-lived ponding events. Such small-scale facies variability, occurring over limited lateral distances, underscores the importance of high-resolution geophysical methods for accurate subsurface characterization.

The recognition of four principal stratigraphic units within the investigated depth of approximately 22 m provides an integrated view of the depositional evolution of the study area. The surficial pebbly sand unit reflects high-energy depositional conditions, likely associated with recent or reworked fluvial processes. The underlying clayey sand and clayey silty sand units indicate a gradual transition to lower-energy environments, with increasing fine-grained content reflecting reduced flow competence and enhanced suspension settling. The basal clayey silt layer represents the lowest-energy depositional phase, potentially linked to lacustrine or distal floodplain settings. Collectively, this vertical succession records a progressive shift in sedimentary regimes, which may be associated with climatic fluctuations, changes in base level, or regional geomorphological evolution during the late Quaternary. Overall, the results highlight the effectiveness of GPR as a non-invasive tool for resolving complex shallow stratigraphy and for interpreting sedimentary processes at both local and site scales. The detailed stratigraphic insights obtained in this study are particularly valuable for hydrogeological assessments, geotechnical investigations, and land-use planning in similar valley-dominated Quaternary terrains.

Conclusion

Ground-penetrating radar (GPR) proved to be an effective and high-resolution technique for delineating shallow subsurface stratigraphy, enabling reliable discrimination between lithological units and subsurface features. In the Bosita district, the acquired GPR data were successfully utilized to estimate the depth to the water table and the configuration of the underlying bedrock surface. Sediment thickness within the surveyed valleys ranges from approximately 2.5 to 6.5 m, with a clear thinning trend toward the valley margins. The interpreted profiles (AB, BC, DA, and AC) reveal a pronounced bedrock ridge that separates adjacent paleo-channels infilled by late Quaternary sediments. At greater depths, the subsurface architecture becomes increasingly complex, characterized by rapid lateral facies transitions associated with interbedded lenses of clay, silt, and sand over short spatial intervals. Overall, the stratigraphic interpretation identifies four principal subsurface units within an investigated thickness of ~22 m: an upper pebbly sand layer, underlain successively by clayey sand, clayey silty sand, and a basal clayey silt layer.

References:

1. Annon, A, P. (2005) Graund Penetration Radar, investigation in geophysics, geophysics, V13. 357-438.
2. Hlal, O and Bennur, S (2014), Sedimentology and Stratigraphy Architecture of the late Pleistocene-Holocene Succession of the Gargaresh Formation, Subratah Basin, NW Libya Geophysical Research Abstracts Vol. 16, EGU2014-14321, 2014.
3. Molron, J., Linde, N., Baron, L., Selroos, J., Darcel, C., & Davy, P. (2020). Which fractures are imaged with Ground Penetrating Radar? Results from an experiment in the Äspö Hardrock Laboratory,Sweden. Engineering Geology, 273, 105674.
4. Neal, A. (2004), 'Ground-penetrating radar and its use in sedimentology: principles, problems and progress', Earth-Science Review 66, 261–330.
5. Tatum, D.I. and Francke, J. (2012) 'Constructing hydrocarbon reservoir analogues of aeolian systems using ground penetrating radar', Journal of Applied Geophysics, 81, pp. 21–28.